CHEMISTRY
AN ASIAN JOURNAL

DOI: 10.1002/asia.200800232

Synthesis, Crystal Structure, Bonding, and Properties of $(Ba_6O)(OsN_3)_2$

Carsten L. Schmidt, Ulrich Wedig, Robert Dinnebier, and Martin Jansen*[a]

Abstract: The new barium nitridoosmate oxide $(Ba_6O)(OsN_3)_2$ was prepared by reacting elemental barium and osmium (3:1) in nitrogen at 815–830 °C. The crystal structure of $(Ba_6O)(OsN_3)_2$ as determined by laboratory powder X-ray diffraction ($R\bar{3}$, No 148: $a=b=8.112(1)$ Å, $c=17.390(1)$ Å, $V=991.0(1)$ Å^3, $Z=3$), consists of sheets of trigonal OsN_3 units and trigonal-antiprismatic Ba_6O groups, and is structurally related to the "313 nitrides" AE_3MN_3 (AE = Ca, Sr, Ba, M = V–Co, Ga). Density functional calculations, using a hybrid functional, likewise indicate the existence of oxygen in the Ba_6 polyhedra. The oxidation state 4+ of osmium is confirmed, both by the calculations and by XPS measurements. The bonding properties of the OsN_3^{5-} units are analyzed and compared to the Raman spectrum. The compound is paramagnetic from room temperature down to $T=10$ K. Between room temperature and 100 K it obeys the Curie–Weiss law ($\mu=1.68$ μ_B). $(Ba_6O)(OsN_3)_2$ is semiconducting with a good electronic conductivity at room temperature (8.74×10^{-2} Ω^{-1}cm^{-1}). Below 142 K the temperature dependence of the conductivity resembles that of a variable-range hopping mechanism.

Keywords: density functional calculations · nitrides · osmium · semiconductors · X-ray diffraction

Introduction

Binary and ternary nitrides have continued to be a field of major interest in solid-state inorganic chemistry.[1–11] Currently, nitrides of the electron-rich transition metals (Ru–Cd, Re–Hg) are attracting particular interest. Recent work, using diamond anvil cells (DACs), claimed the synthesis and characterization of several binary nitrides starting from the elements.[12–14] Among those OsN_2, and the hypothetical OsN have been studied theoretically.[15–21] Nitrides of osmium are expected to be possible superhard materials since the bulk modulus of the element is already very high.[22] While "OsN" has remained elusive so far, OsN_2 (osmium diazenide) has been synthesized.[14] The reaction of elemental osmium with N_2 has been stated to occur above 50 GPa and 2000 K, yielding OsN_2 with dinitrogen moieties inserted into the Os lattice. However, no fully convincing structural solution has been provided and no independent analytical probe (elemental analysis, spectroscopy) has been employed to support the proposed model. Therefore, from a general point of view, more confirmed structural as well as chemical information on osmium nitrides is highly desirable. Since all binary nitrides of osmium were calculated to be metastable or unstable at ambient pressure, we have focused on the preparation of ternary nitrides. Electropositive metals (alkali and alkaline earth metals) stabilize the transition-metal–nitrogen bond owing to weak counterpolarization, the same phenomenon might also be rationalized based on common acid–base concepts.[23,24] Besides the well-known nitride-oxoosmates which contain the anion OsO_3N^- (however, frequently incorrectly called nitridoosmates) the existence of ternary nitridoosmates has been mentioned only once thus far,[25] without giving structural details. Intending to synthesize barium nitridoosmates from the metals in a flow of purified nitrogen, we have obtained the first nitridoosmate $(Ba_6O)(OsN_3)_2$, which, however, contains oxygen in the cationic substructure.

[a] C. L. Schmidt, Dr. U. Wedig, Prof. Dr. R. Dinnebier, Prof. Dr. M. Jansen
Max Planck Institute for Solid State Research
Heisenbergstrasse 1, 70569 Stuttgart (Germany)
Fax: (+49) 711 689 1502
E-mail: M.Jansen@fkf.mpg.de

Supporting information for this article is available on the WWW under http://dx.doi.org/10.1002/asia.200800232.

Results and Discussion

The nitridoosmate $(Ba_6O)(OsN_3)_2$ has been synthesized from the metallic elements in a flow of dry nitrogen. At a Ba/Os ratio of 3:1, the system is sensitive to traces of oxygen, and though the reactions were performed in a flow of highly pure (see Experimental Section) nitrogen, oxygen

 © 2008 Wiley-VCH Verlag GmbH & Co. KGaA, Weinheim

was always incorporated in the product. The composition was confirmed by EDX analysis, proving the Ba/Os ratio to be 3:1, and nitrogen and oxygen to be present. By hot-gas extraction, the contents of oxygen and nitrogen (three independent experiments) were directly determined to be 0.82 (calcd 1.23) wt%, and 6.6 (calcd 6.44) wt%, respectively. Considering the intricacies connected to the direct analyses of oxygen and nitrogen, and the limited precision achievable, the results obtained support the composition assumed.

The crystal structure of $(Ba_6O)(OsN_3)_2$ was determined by X-ray powder diffraction. The experimental powder pattern and the Rietveld profile fit are presented in Figure 1, and

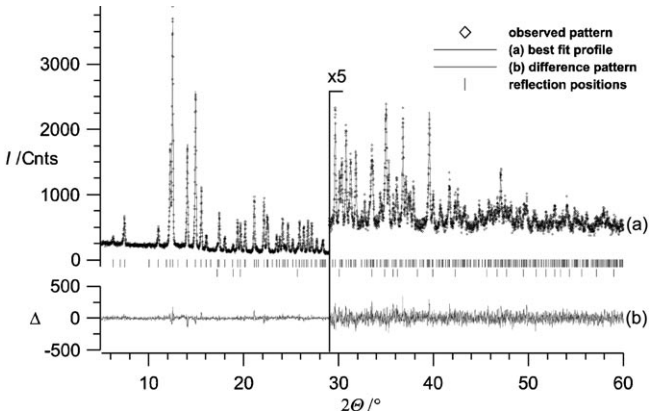

Figure 1. Powder X-ray diffraction pattern of $(Ba_6O)(OsN_3)_2$. As a minor impurity phase elemental osmium was present (3 wt%).

the pertinent crystallographic data are compiled in Tables 1–3. Parts of the structure are shown in Figure 2 and Figure 3. The structural principle of $(Ba_6O)(OsN_3)_2$ is remarkable as both the cationic and anionic parts consist of complex building units, the $[Ba_6O]^{10+}$ metallocomplex[26] and the complex anion OsN_3^{5-}. The cationic $[Ba_6O]$ complex is of trigonal-antiprismatic shape, with the central oxygen atom exhibiting $\bar{3}$ site symmetry (3*b*). The Ba–O distance of 2.73 Å is close to

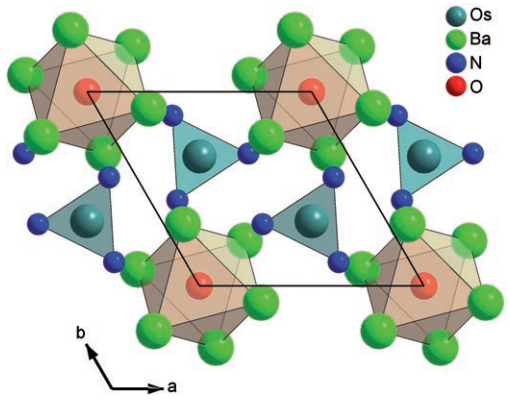

Figure 2. Layers ($\Delta z = 1/6$) of $[Ba_6O]^{10+}$ trigonal antiprisms and trigonal-planar OsN_3^{5-} anions in $(Ba_6O)(OsN_3)_2$. The anions are located alternatively at the bottom and the top of the layer.

the sum of the respective ionic radii (2.76 Å).[27] In addition to this shortest contact, barium is coordinated by five nitrogen atoms, at distances ranging from 2.84 Å to 3.17 Å. Electropositive elements like the alkali metals or alkaline earth metals have been frequently found to coordinate a nonmetal, for example, O, N, or S, octahedrally or tetrahedrally.[26,28,29] The anionic OsN_3^{5-} complex is trigonal (virtually planar) with the central Os atom exhibiting 3 site symmetry (6*c*). Although trigonal-planar, isolated anions of general composition TN_3^{x-} (T = transition metal) have been observed many times,[30] it has been realized here for the first time for osmium. The rather short Os–N bond length of 1.77 Å indicates significant contributions of π bonding. A comparable length, 1.74 Å, has been reported for the imido complex $[Os(NAr)_3]$ (Ar = 2,6-diisopropylphenyl), containing an osmium–nitrogen double bond, while in the μ-nitrido complex $[Os_2N(S_2CNMe_2)_5]$ the Os–N bond length amounts to 1.76 Å.[31,32]

The isolated $[Ba_6O]^{10+}$ antiprisms form a hexagonal layer perpendicular to the crystallographic *c* axis with the OsN_3^{5-} anions located in the two trigonal cavities alternatingly at the bottom and the top of the respective layer (Figure 2). Successive layers are packed in ABC sequence with a shift of 2/3 1/3 1/3 each (Figure 3) following rhombohedral sym-

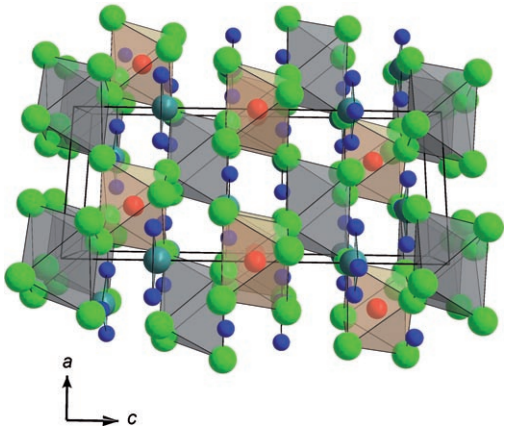

Figure 3. The layers described in Figure 2 are packed in ABC sequence with a shift of 2/3 1/3 1/3 each. The empty trigonal antiprisms between these layers, each formed by six Ba atoms, are drawn in transparent gray.

metry. As a consequence of this packing, Ba atoms of adjacent layers also form trigonal antisprisms. These Ba_6 polyhedra are empty and are connected to the oxygen-filled antiprisms through edges. The volume of the empty polyhedron (center at Wyckoff position 3*a*) is 20% larger than that of the filled one.

If the hexagonal layer described above is cut in half and oxygen is omitted, the remaining sheets of OsN_3 units and triangles of Ba exhibit a striking similarity to the layered arrangement of the atoms in so-called 313 nitrides AE_3MN_3 (AE = Ca, Sr, Ba; M = V–Co, Ga).[33–37] Compared to the stacking of the layers in $(Ba_6O)(OsN_3)_2$ described above,

 © 2008 Wiley-VCH Verlag GmbH & Co. KGaA, Weinheim

however, the Ba partial structure, for example, in Ba_3FeN_3,[33] consists of face-sharing trigonal antiprisms, an arrangement which is unfavorable to accommodate ionic species. The presence of filled Ba_6 polyhedra in $(Ba_6O)(OsN_3)_2$ induces the different stacking pattern, thus avoiding face sharing. Seemingly, the structures adapt to the compositions as determined by the chemical nature of the constituents, while optimizing the electrostatic contribution to the lattice energy. As the Ba_6 polyhedra shrink upon filling with oxygen, the packing factor[38] of $(Ba_6O)(OsN_3)_2$ (49.2%) is larger than in Ba_3FeN_3 (47.1%).

The impact of the Ba partial structure to stabilize the Os compound is confirmed by hybrid functional DFT calculations. Computed structural parameters, selected distances, and charges, considering different fillings of the Ba_6 polyhedra, are compiled in Table 4. If the trigonal antiprisms are assumed to be vacant, the computed structures exhibit equally sized polyhedra and equidistant layers. The same is true for the variant where all these voids are completely filled by oxygen. Astonishingly the lattice constants change only very slightly upon complete filling, pointing to only minor changes of the overall ionic interactions. The varying size of the Ba_6 voids, which is observed experimentally, as well as the lattice constants are best reproduced by calculations where oxygen atoms are inserted at Wyckoff position 3*b* (0, 0, $^1/_2$), thus filling half of the voids, although the alternation of the interlayer distances is overestimated in this case. Substituting O by N leads to a more pronounced alternation and to a *c* parameter which is too large by 0.21 Å.

The Ba_6 voids play a special role in the structure. Although it is difficult to deduce formal charges from the results of a Mulliken population analysis, it is obvious that a significant amount of charge has to be attributed to the basis functions centered in the void, $-0.7\,e^-$ in the empty $(Ba_6\square)(OsN_3)_2$ (see Table 4). The calculations clearly show a spin polarization ($-0.6\,e^-$) of this charge. According to the band structures, or the densities of states (DOS) as their integrated form (Figure 4), this charge is caused by two spin bands, that is, singly occupied bands of either spin channel. These bands are located below the Fermi level together with two spin bands with π character per OsN_3 unit (black part of the DOS in Figure 4). Whereas the latter are narrow, the width of the spin bands associated with the voids depends on the spin density. In the case of the upper diagram in Figure 4, the spin densities at the Os sites are of equal sign; those in both voids have opposite sign. The width of the spin bands attributed to the voids is 0.08 Hartree. In the case where the sign of the spin density alternates between adjacent layers (second diagram in Figure 4), only a narrow peak is found in the DOS at $E=-0.1$ H. This dependence of the bandwidth on the spin coupling makes it difficult to predict the width of the band gap for the empty $(Ba_6\square)(OsN_3)_2$. Apart from this uncertainty, structural details and partial charges of both spin variants do not differ significantly, as mentioned in the methods section, and the difference of the total energies is only 11 kJ mol^{-1}. Taking the electrons being trapped in the Ba_6 voids into account, an oxidation state of 4+ has to be attributed to Os for this hypothetical composition $(Ba_6\square)(OsN_3)_2$.

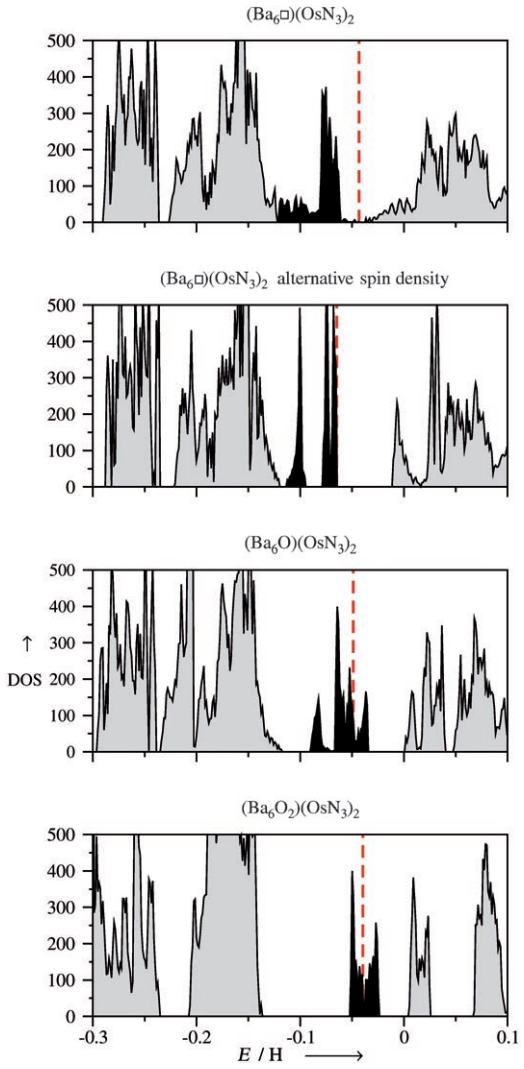

Figure 4. Total densities of states (DOS [states H^{-1} cell^{-1}]) of $(Ba_6\square)(OsN_3)_2$ (first and second diagram from top to bottom show two different configurations of the spin density), $(Ba_6O)(OsN_3)_2$ with O at Wyckoff position 3*b* (third diagram), and $(Ba_6O_2)(OsN_3)_2$ with O at Wyckoff positions 3*b* and 3*a* (fourth diagram). The black areas in the DOS near the Fermi level are discussed in the text in more detail.

With the filling of the voids at Wyckoff position 3*b* by oxygen atoms, the corresponding spin bands become more localized and are shifted to lower energies. That is why we find within the primitive cell only one spin band associated with the remaining empty void together with four *e* bands of the OsN_3 units at the Fermi level (black area in the third diagram in Figure 4). These five spin bands are occupied by only four electrons, leading to a nonzero DOS at the Fermi level. Owing to the uncertainty concerning the width of specific bands at E_F discussed above, an unambiguous interpretation is not possible. However, the only slight decrease of the spin charge at the OsN_3 unit (1.6) suggests that the oxidation state of Os in $(Ba_6O)(OsN_3)_2$ is the same as in the empty variant. If nitrogen is substituted for oxygen [(Ba_6N)-

 © 2008 Wiley-VCH Verlag GmbH & Co. KGaA, Weinheim

$(OsN_3)_2$] or if oxygen is incorporated in both positions, 3*a* and 3*b* [$(Ba_6O_2)(OsN_3)_2$], the reduced spin charge, however, would indicate a higher oxidation state of Os.

Although the agreement of the computed structure with the experimental data is best for the composition $(Ba_6O)(OsN_3)_2$, a partial substitution of O by N cannot be ruled out. Unfortunately, X-ray powder diffraction also does not unambiguously discriminate oxygen and nitrogen, especially not if they are included in a heavy atom matrix. As the nature of the atom in the Ba_6 antiprisms directly affects the valency of Os, XPS can give further hints on the real composition. For the XPS studies, elemental osmium and osmium(IV) oxide were selected as references since no data on nitrides are available so far, and also oxygen is more similar to nitrogen than any other ligand, for example, with respect to electronegativity or π bonding. After sputtering, the Os $4f_{7/2}$ and $4f_{5/2}$ peaks were recorded at 52.0 eV and 54.7 eV, respectively. These values match well with the data published for OsO_2 (51.7 eV and 54.2 eV[39]). After long sputtering, additional Os lines emerged at 50.5 eV and 53.4 eV, corresponding to elemental osmium. This indicates partial decomposition and provides additional reference lines. The Ba lines were observed at 779.3 eV ($3d_{5/2}$) and 794.7 eV ($3d_{3/2}$). They do not change even after sputtering and correspond to the published values 779.1 eV ($3d_{5/2}$) and 794.2 eV ($3d_{3/2}$) for BaO.[40] The N(1s) photoelectron signal appears as an asymmetric peak, resulting from a superposition of two lines at 396.4 eV and 398.1 eV. Similar asymmetries of the N(1s) line have been reported to occur for layered materials like the binary alkaline earth subnitrides AE_2N or Cs_2O (asymmetric O(2p) line).[41] The position of the N(1s) peak is indicative for covalent bonding as observed in metal organic compounds or binary transition-metal nitrides.[42]

Assuming an oxidation state of 4+ for osmium, the bonding in the complex anion OsN_3^{5-} can be illustrated on the basis of extended Hückel (EH) molecular orbitals (MOs) of the isolated anion (D_{3h} symmetry, Figure 5). The lowest-valence orbitals, 3a1′ and 3e′, mainly consist of the N 2s atomic orbitals (AOs). The admixture of Os AOs is very low and the orbital energies are even shifted slightly upwards compared to the N 2s AOs. These molecular orbitals of σ character have to be regarded as nonbonding. The next set of doubly degenerate orbitals, 1e″ and 4e′, comprises combinations of Os $5d_{xz}$ and $5d_{yz}$ (1e″) and of Os $5d_{xy}$ and $5d_{x^2-y^2}$ (4e′) with the corresponding N 2p orbitals. These MOs are definitely bonding out-of-plane (1e″) and in-plane (4e′) π-type molecular orbitals. The following 1a2′ and 2a2″ orbitals are nonbonding, consisting only of N 2p AOs. The set of 5e′ and 4a1′ includes combinations of Os $5d_{xy}$ and $5d_{x^2-y^2}$ (5e′) and Os $5d_{z^2}$ (4a1′) with the related N 2p AOs, however, without energy gain at the EH level, indicating a nonbonding character. The 5a1′ molecular orbital is a combination of the Os 6s orbital with N 2p AOs. The significant contribution of the s-valence orbital in trigonal-planar transition-metal units seems to be characteristic. This phenomenon was related, for example, to the unusual negative Mössbauer isomer shift in Ba_3FeN_3.[43] The bonding contribution of the 5a1′ MO, relative to the Os 6s AO, is compensated by the antibonding character of the half-filled doubly degenerate HOMO (2e″). At the EH level, bonding and antibonding contributions thus sum up to a bond order of 1.3.

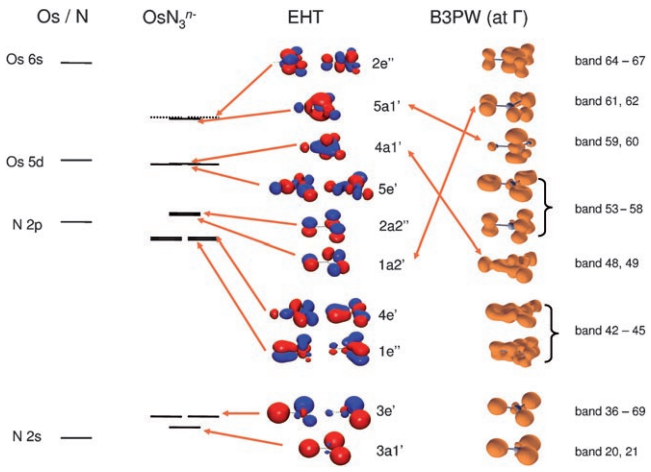

Figure 5. EH terms and molecular orbitals of the isolated OsN_3^{5-} anion as well as sections at the OsN_3^{5-} anion of the electron densities computed from the Kohn–Sham eigenfunctions at the Γ point in the Brillouin zone.

A comparison of this simple EH picture with the results from the hybrid functional DFT calculations for the crystal reveals an astonishingly good agreement. Sections at the OsN_3^{5-} anion of the electron densities computed from the Kohn–Sham eigenfunctions at the Γ point in the Brillouin zone exhibit the same characteristic as the EH molecular orbitals (Figure 5). Moreover, the order of the eigenvalues is the same overall, with the exception that the bands associated with the 4a1' and 5a1' MOs are shifted downward. Whereas the stabilization of the 4a1' band may be related to a higher bond order in the OsN_3^{5-} unit at the DFT level, the down shift of the 5a1' band is caused by an interaction with the 2p orbitals of oxygen atoms in the Ba_6 polyhedra, coupling the spins at different Os sites.

The structural findings derived so far were further substantiated by spectroscopy. In the Raman spectrum (Figure 6), a strong band at 748 cm^{-1} and a very weak band at 1058 cm^{-1} were noticeable. Moreover, there is a hump at 390 cm^{-1}. These Raman data reflect the D_{3h} symmetry of the OsN_3^{5-} anion,[44] which is expected to produce the fundamental vibrations A_1' (ν_s) and $2\times E'$ (ν_{as} and δ). We assign the intense Raman line at 748 cm^{-1} to ν_s, the weak one at 1058 cm^{-1} to ν_{as}, and the feature at 390 cm^{-1} to δ.

The magnetic properties of the material were analyzed and paramagnetic behavior was observed from room temperature down to $T=10$ K. At room temperature, the molar magnetic susceptibility χ_{mol} is 6.84×10^{-4} cm^3mol^{-1}. In the temperature range from 98 K up to 300 K the temperature dependence of the reciprocal magnetic susceptibility has been fitted according to the Curie–Weiss law, with a Weiss constant $\Theta=-207.6(5)$ K and a Curie constant $C=0.3534(5)$ $cm^3\,K\,mol^{-1}$ (Figure 7). The corresponding magnetic moment of 1.68 μ_B is rather low for an ion with two un-

 © 2008 Wiley-VCH Verlag GmbH & Co. KGaA, Weinheim

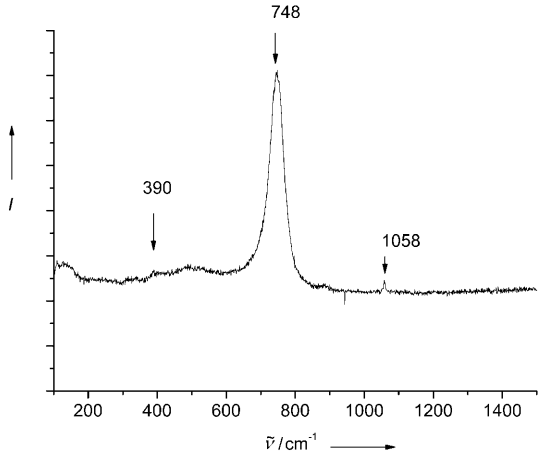

Figure 6. Raman spectrum of $(Ba_6O)(OsN_3)_2$.

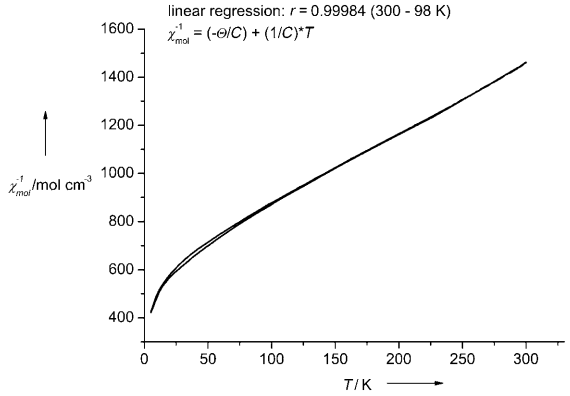

Figure 7. Fitting the data of the magnetic measurement. Curie–Weiss behavior was observed down to 98 K.

paired electrons, yet typical for Os^{4+} (e.g., 1.51 μ_B in K_2OsCl_6[45]). To understand the magnetic behavior, further investigations including the coupling via the oxygen 2p orbitals are necessary.

Concerning the specific electrical resistivity, the complex oxide nitride showed semiconducting behavior in the temperature range considered from 50 K to 300 K (Figure 8). At

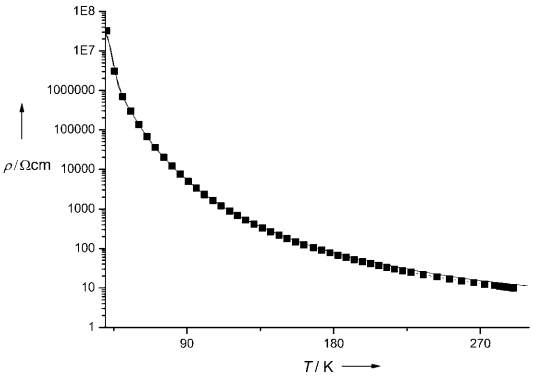

Figure 8. The specific electrical resistivity of $(Ba_6O)(OsN_3)_2$ as a function of temperature.

temperatures $T<50$ K, the resistivity was rather high ($>1.0\times10^6\,\Omega$ cm) while at 300 K (RT) the value for the conductivity was found to be $8.74\times10^{-2}\,\Omega^{-1}\,cm^{-1}$. In the range from 300 K to 135 K, the temperature dependence of the conductivity could be analyzed according to the Arrhenius model with an activation energy (E_a) of 7.19 kJ mol^{-1} (0.074 eV). This rather low E_a value is in accordance with the black color of the material and the good electronic conductivity at room temperature. At temperatures below $T=$ 142 K the specific conductivity can be described by a $T^{-1/3}$ law (GoF = 0.99976). Such a temperature dependence is obtained with a variable-range hopping model (VRH) in anisotropic disordered systems with localized states.[46] The computed residual spin density in the empty Ba_6 polyhedra, associated with a band at the Fermi level, may be related to an analogous conduction mechanism.

Conclusions

In this study we present $(Ba_6O)(OsN_3)_2$, the first structurally characterized nitridoosmate. Using several complementary analytical techniques, composition, chemical bonding, and physical properties of the compound have been investigated. Concerning the general topology as well as the primary building blocks, the material is exhibiting similarities to the known hexagonal 313 nitrides AE_3MN_3. However, in contrast to Ba_3FeN_3, where iron is in the oxidation state of 3+, the osmium in the trigonal, virtually planar OsN_3 unit adopts the oxidation state 4+, which was confirmed by photoelectron spectroscopy and density functional calculations. The electron additionally provided by osmium has to be assigned to the barium partial structure, leading in the presence of small amounts of oxygen to the formation of a $[Ba_6O]^{10+}$ cationic complex. The unique arrangement of filled and empty Ba_6 trigonal antiprisms in the paramagnetic compound $(Ba_6O)(OsN_3)_2$ induces a semiconducting behavior with a low activation barrier and VRH-like conduction mechanism at low temperatures. We are aware that none of the methods applied gives final certainty concerning the stoichiometric and ordered arrangement of oxygen in half of the Ba_6 voids. As this uncertainty only affects the Ba partial structure, it does not influence the conclusions drawn, especially concerning the overall structure, the oxidation state of Os, and the bonding properties of the OsN_3 unit.

Experimental Section

Synthesis

$(Ba_6O)(OsN_3)_2$ was prepared from the elements under an atmosphere of N_2 (Westfalen, quality 5.0, passed over standard drying towers and an oxysorb catalyst). Finely cut slices of elemental barium (distilled and stored under argon and subsequently heated in a sealed Ta ampoule at $T>800$ °C under dynamic vacuum to remove traces of hydrogen) were mixed with dried osmium powder ($T=400$ °C, 10^{-3} mbar, 12 h) in a ratio of 3:1. The mixture was placed in a predried tantalum crucible ($T=$ 1100 °C, 10^{-6} mbar, 12 h) which was transferred into a quartz tube (dried

 © 2008 Wiley-VCH Verlag GmbH & Co. KGaA, Weinheim

at $T=900\,°C$, 10^{-3} mbar, 12 h) and heated up to $T=800\,°C$ for 10 h in a flow of nitrogen. After grinding the pretreated mixture, the black powder was annealed again at $T=800\,°C$ for 50 h. X-ray powder diffraction studies at this stage showed that the product contained elemental Os and Ba_2N. Subsequently, the powder was reground and annealed for 30 h at $T=815\,°C$, 820 °C and 825 °C. After this treatment, Ba_2N was no longer detectable by X-ray powder diffraction. The black product was sensitive to moisture.

X-ray Powder Diffractometry

X-ray powder diffraction data of $(Ba_6O)(OsN_3)_2$ were collected at room temperature with a Stoe Stadi-P transmission diffractometer (primary beam Johannson type Ge monochromator for $Mo_{K\alpha1}$ radiation, linear PSD) with the sample sealed in a borosilcate-glass capillary of 0.3 mm diameter. The powder pattern was recorded for 20 h in the range 2–60° 2θ with a step width of 0.01° 2θ using a linear position-sensitive detector with an opening of approximately 12° 2θ. The sample was spun during measurement for better particle statistics. The powder pattern contains a few weak reflections of elemental osmium. Further experimental details are given in Table 1. Indexing[47] led to an R-centered trigonal unit cell

Table 1. Crystallographic data for $(Ba_6O)(OsN_3)_2$.

	$(Ba_6O)(OsN_3)_2$
Space group	$R\bar{3}$(No. 148)
Cell parameters [Å]	$a=8.112(1)$
	$c=17.390(1)$
Cell volume [Å^3]	$V=991.0(1)$
Z	3
T [K]	300
Formula weight [g mol^{-1}]	1304.48
ρ_{calcd} ($\rho_{measured}$) [g cm^{-3}]	6.56 (6.46)
Radiation source [Å]	$\lambda=0.7093$
R_{exp} [%][a]	2.76
R_{wp} [%][a]	6.65
R_p [%][a]	5.67
R_{Bragg} [%][a]	1.78
GoF	2.408

[a] as defined in TOPAS.

with lattice parameters given in Table 1. The number of formula units per unit cell could be determined to be $Z=3$ from volume increments assuming a Ba/Os ratio of 3:1. The extinctions found in the powder patterns indicated either $R3$, $R\bar{3}$, $R32$, $R3m$, or $R\bar{3}m$ as possible space groups, of which $R\bar{3}$ could later be confirmed by Rietveld refinement.[48] Structure determination and refinement was performed using the program TOPAS Version 3.0 (Bruker AXS, 2007). The peak profiles and precise lattice parameters were determined by a LeBail fit[49] using the fundamental parameter approach of TOPAS.[50] A simulated annealing run[51] using a merging radius of 0.6 Å for Os, Ba, and N immediately found the atomic positions for these elements. A consecutive Rietveld refinement converged to a Bragg R value of 1.7% (Figure 1). For verification of the trigonal-planar environment of the osmium cation, three alternatives, also satisfying the threefold axis (tetrahedral OsN_4, trigonal-bipyramidal OsN_5, and octahedral OsN_6) were tested, all leading to a significantly worse reliability factor. Placing an oxygen atom in the center of the Ba_6 trigonal antiprisms (3*b*, 0,0,0.5) yielded a significantly better profile R value. Quantitative phase analyses by the Rietveld method lead to a fraction of 3 wt% of elemental osmium. Agreement factors (R values) are listed in Table 1, the coordinates are given in Table 2, and a selection of interatomic distances and angles is given in Table 3. Using the programs Platon[52] and K-plot,[53] no additional symmetry could be detected. It is worth noting that the sample after exposing it to a synchrotron beam (ESRF, beamline ID31, wavelength of 0.3 Å) had decomposed into elemental osmium and an unknown amorphous phase.

Further details of the crystal structure investigation can be obtained from the Fachinformationszentrum Karlsruhe, 76344 Eggenstein-Leopoldshafen, Germany (fax: (+49)7247-808-666; email: crysdata@fiz-karlsruhe.de) on quoting the depository number CSD-419467

Table 2. Atomic positions and isotropic thermal parameters of $(Ba_6O)(OsN_3)_2$.

Atom	Wyck.	x	y	z	U(eq) [Å^2]
Ba	18*f*	0.317(3)	0.231(2)	0.416(4)	0.58(2)
Os	6*c*	0	0	0.247(8)	0.58(2)
N	18*f*	0.210(7)	0.225(9)	0.240(4)	0.71(4)
O	3*b*	0	0	0.5	0.71(4)

Table 3. Selected bond lengths [Å] and angles [°] for $(Ba_6O)(OsN_3)_2$.

Os–N	1.77(8)
Os–Ba	3.46(3)
	3.73(1)
	3.81(9)
Ba–N	2.84(1)
	2.87(7)
	2.88(4)
	3.16(9)
	3.17(4)
Ba–O	2.72(7)
Ba–Ba	3.71(2)
	3.83(7)
	4.00(0)
N–Os–N	119.5(0)

Raman Spectroscopy

For the Raman experiments the powdered sample was filled in a 1.0 mm lithium borate glass capillary (Hilgenberg, glass No 14). The measurement was performed with an excitation line of 632.817 nm (Labram 010, single grating). The acquisition time was 5 to 300 s with a laser power between 0.4 and 0.004 mW.

Electrical Conductivity Measurements

Measurements were performed on compacted polycrystalline powder pellets (diameter 5 mm, thickness 0.8 mm, pressed with 920 MPa) using the standard four-point technique.

Energy-Dispersive X-ray Analysis

EDX analysis was performed on an XL30 TMP (Philips Electron Optics GmbH). An energy-dispersive detector S-UTW(Li) (EDAX) was used. The powder sample stored in a glovebox filled with argon was placed on a sample holder. The sample was attached to the spectrometer through a transfer chamber, providing inert conditions.

Quantitative Elemental Analysis

For the simultaneous determination of the elements N and O, a hot-gas extraction analysis was performed (model TC-436, Fa. LECO). The substance (10–20 mg) was filled in a tin crucible, and small amounts of elemental tin and nickel were added. The sample was transferred under He in a preheated graphite crucible ($T=2500$ K). Oxygen was identified as CO_2 (IR spectroscopy), nitrogen as elemental N_2 (thermal conductivity). Reference materials used were SiO_2 and Si_3N_4.

Magnetic Measurements

Magnetic susceptibilities were measured using an MPMS7 SQUID Magnetometer (Quantum design) between 2 and 300 K. Powder samples were filled in Suprasil quartz glass tubes filled with helium. The data were corrected for the magnetization of the empty sample holder and for the diamagnetic contributions of the constituent ions by fitting the data according to $\chi_g(\text{corr.})=\chi_g-\chi_0$; χ_0 was obtained by fitting the experimental data to $\chi_g=\chi_0+C_g/(T-\theta)$.

XPS Measurements

ESCA (electron spectroscopy for chemical analysis) spectra were recorded on an electron spectrometer (AXIS ULTRA, Kratos Analytical) by use of monochomated $Al_{K\alpha}$ radiation (1486.58 eV). The vacuum during the measurement was kept at about 3×10^{-9} Torr. The sample was prepared in an argon-filled glovebox and transferred to the spectrometer by a chamber providing inert conditions. The sample surface was sputtered with high-purity argon for 1–18 min (Ar^+, 1 kV). To account for charg-

 © 2008 Wiley-VCH Verlag GmbH & Co. KGaA, Weinheim

ing, the spectra were calibrated with respect to an internal C(1s) line (binding energy 284.60 eV).

Quantum Chemical Calculations

All quantum mechanical calculations were performed with the CRYSTAL06 program[54] using local Gaussian basis functions and scalar-relativistic pseudopotentials to describe the inner-core electrons. Structures and bands were analyzed by means of the XCrySDen program.[55] The following pseudopotentials and basis sets were selected. Os: small core, 16 valence electrons with a [4s/5p/2d] basis set.[56] To comply with the requirements of the CRYSTAL code for periodic systems, the parameter set given was truncated by omitting the g projection of the semilocal pseudopotential as well as the most diffuse basis functions. Ba: 10 valence electrons, including 5s and 5p in the SCF process, with a [3s/3p/1d] basis set.[57] The parameters of the f projection were used as local part of the pseudopotential and subtracted from the projections for $l=0$ to 2. The two most diffuse s and p functions of the basis set given in reference [57] were replaced by a single sp shell with the exponent $\eta=0.08$. The exponent of the single d function was set to $\eta=0.4$. N, O: 5 and 6 valence electrons with a [2s/2p] basis, respectively.[58] The third p function of oxygen, given in reference [58], was left out. In the course of the investigations it was found that a Ba-centered basis set is not sufficient to describe the electron density within the empty voids formed by the Ba_6 trigonal antiprisms. Therefore two sp shells ($\eta=$ 0.4 and 0.15) and one d shell ($\eta=0.2$) were positioned in the middle of the voids. For the same reason, the basis sets of the oxygen and nitrogen atoms located at these sites were augmented by one sp shell ($\eta=0.15$) and one d shell ($\eta=0.2$).

For the DFT calculations presented here we applied the hybrid functional B3PW, which corresponds to the B3LYP ansatz,[59] except for the Perdew–Wang nonlocal correlation part.[60] Lattice constants and atomic positions were optimized simultaneously using the default convergence criteria (gradient: 0.0003 a.u. (RMS) and 0.00045 a.u. (largest component); estimated displacement: 0.0012 a.u. (RMS) and 0.0018 a.u. (largest component)). The single energy calculations were converged to 10^{-7} H. The eigenvalues were evaluated at 40 **k** points in the irreducible part of the Brillouin zone. To compute the Fermi energy and the density matrix, a denser net (294 **k** points) was used.

In all calculations spin polarization was taken into account. The structural data presented here all refer to results for the crystallographic space group $R\bar{3}$ with the same spin density at all Os sites. Additional calculations were performed without inversion symmetry to allow for spin densities of opposite sign at the Os sites in adjacent layers. This type of calculation showed a worse energy convergence behavior during the structure optimization procedure, which could be resolved by a so-called temperature smearing of the Fermi surface, where the occupancy of the eigenvalues is computed from the Fermi function instead of the step function. The energy of the system obtained in this way had to be extrapolated to $T=0$ K to be comparable to results computed without temperature smearing. The uncertainty of this extrapolation, however, is on the order of magnitude like the energy difference of states with different spin arrangement. The optimized structural data and the charge distribution of a particular composition are less affected by variations in the spin configuration. The largest deviations from the values in Table 4 for the *a*-lattice parameter, the *c*-lattice parameter, the distances, and the partial and spin charges are 0.01 Å, 0.08 Å, 0.02 Å, 0.01 e^-, and 0.1 e^-, respectively. Hence the data presented in Table 4 can be regarded as representative.

Table 4. Experimental and calculated lattice constants [Å] of $(Ba_6E_x)(OsN_3)_2$ (E = □, O, N), as well as distances [Å], binding energies [kJ mol^{-1}], and partial and spin charges.

	Exptl $(Ba_6O)(OsN_3)_2$	Calcd $(Ba_6□)(OsN_3)_2$	$(Ba_6O)(OsN_3)_2$	$(Ba_6N)(OsN_3)_2$	$(Ba_6O_2)(OsN_3)_2$
Wyck. pos. 3*b*	O	–	O	N	O
Wyck. pos. 3*a*	–	–	–	–	O
Lattice constants					
a	8.112	8.077	8.085	8.135	8.094
c	17.390	17.348	17.414	17.599	17.359
Distances					
Ba Wyck. 3*b*	2.73	2.82	2.71	2.70	2.80
Ba Wyck. 3*a*	2.91	2.82	2.92	2.96	2.80
Ba–Ba (around 3*b*)	3.71/4.00	3.77/4.20	3.65/4.01	3.66/3.98	3.76/4.15
Ba-Ba (around 3*a*)	3.84/4.37	3.77/4.20	3.90/4.36	3.95/4.40	3.76/4.16
interlayer (Ba)	2.89/2.91	2.89	2.83/2.96	2.84/3.02	2.89
Os–N	1.78	1.88	1.86	1.84	1.82
Binding energies					
atoms in Ba_6 voids			822	578	1586
Partial charges					
$OsN_3^{\delta-}$		−2.8	−2.6	−2.4	−2.4
Ba		+1.2	+1.3	+1.4	+1.4
Wyck. pos. 3*b*		−0.7	−1.9	−2.8	−1.8
Wyck. pos. 3*a*		−0.7	−0.5	−0.5	−1.8
Spin charges					
$OsN_3^{\delta-}$		+1.9	+1.6	+1.1	+1.0
Ba		−0.1	+0.1	+0.1	0
Wyck. pos. 3*b*		−0.6	0	0	0
Wyck. pos. 3*a*		−0.6	+0.5	+0.4	0

The binding energies of the O and N atoms inserted in the voids of the Ba_6 trigonal antiprisms were calculated as the difference between the minimal energy of the filled variant and the sum of the minimal energy of the empty structure and the atomic energy of the incorporated atom. The latter was evaluated by considering all basis functions in a sphere with $R=5.6$ Å around the respective atom, thus accounting for the basis set superposition error. Binding energies as well as the band structures discussed above refer to the primitive cell. The atomic charges are obtained from a Mulliken population analysis. No charges are given for the Os and N atoms, but only for the OsN_3 unit (Table 4). Owing to the short Os–N distance, an atomic partitioning according to the Mulliken scheme would be highly dependent on the basis set.

Acknowledgements

We thank M. Konuma for performing the ESCA measurements, and E. Brücher and G. Siegle for measuring the magnetic and the conductivity data. Support by the Fonds der Chemischen Industrie (FCI) and the German National Merit Foundation (scholarships for C.L.S.) is gratefully acknowledged.

[1] R. Juza, K. Langer, K. von Benda, *Angew. Chem.* **1968**, *80*, 373; *Angew. Chem. Int. Ed. Engl.* **1968**, *7*, 360.
[2] N. E. Brese, M. O'Keeffe, *Struct. Bonding (Berlin)* **1992**, *79*, 307.
[3] W. Schnick, *Angew. Chem.* **1993**, *105*, 846; *Angew. Chem. Int. Ed. Engl.* **1993**, *32*, 806.
[4] R. Metselaar, *Pure Appl. Chem.* **1994**, *66*, 1815.
[5] R. B. King, *Can. J. Chem.* **1995**, *73*, 963.
[6] R Niewa, H. Jacobs, *Chem. Rev.* **1996**, *96*, 2053.
[7] F. J. DiSalvo, S. J. Clarke, *Curr. Opin. Solid State Mater. Sci.* **1996**, *1*, 241.
[8] A. Simon, *Coord. Chem. Rev.* **1997**, *163*, 253.

 © 2008 Wiley-VCH Verlag GmbH & Co. KGaA, Weinheim

[9] R. Kniep, *Pure Appl. Chem.* **1997**, *69*, 185.
[10] R. Niewa, F. J. DiSalvo, *Chem. Mater.* **1998**, *10*, 2733.
[11] D. H. Gregory, *Coord. Chem. Rev.* **2001**, *215*, 301.
[12] E. Gregoryanz, C. Sanloup, M. Somayazulu, J. Badro, G. Fiquet, H.-K. Mao, R. J. Hemley, *Nat. Mater.* **2004**, *3*, 294.
[13] J. C. Crowhurst, A. F. Goncharov, B. Sadigh, C. L. Evans, P. G. Morrall, J. L. Ferreira, A. J. Nelson, *Science* **2006**, *311*, 1275.
[14] A. F. Young, C. Sanloup, E. Gregoryanz, S. Scandolo, R. J. Hemley, H.- K. Mao, *Phys. Rev. Lett.* **2006**, *96*, 155501.
[15] J. A. Montoya, A. D. Hernandez, C. Sanloup, E. Gregoryanz, S. Scandolo, *Appl. Phys. Lett.* **2007**, *90*, 11909.
[16] R. Yu, Q. Zhan, L. C. De Jonghe, *Angew. Chem.* **2007**, *119*, 1154; *Angew. Chem. Int. Ed.* **2007**, *46*, 1136.
[17] J.-C. Zheng, *Phys. Rev. B* **2005**, *72*, 052105.
[18] C.-Z. Fan, S.-Y. Zeng, L.-X. Li, Z.- J. Zhan, R.-P. Liu, W.- K. Wang, P. Zhang, Y.-G. Yao, *Phys. Rev. B* **2006**, *74*, 125118.
[19] Z. Wu, X. Hao, X. Liu, J. Meng, *Phys. Rev. B* **2007**, *75*, 054115.
[20] Z. W. Chen, X. J. Guo, Z. Y. Liu, M. Z. Ma, Q. Jing, G. Li, X. Y. Zhang, L. X. Li, Q. Wang, Y. J. Tian, R. P. Liu, *Phys. Rev. B* **2007**, *75*, 054103.
[21] Y. X. Wang, M. Arai, T. Sasaki, *Appl. Phys. Lett.* **2007**, *90*, 61922.
[22] H. Cynn, J. E. Klepeis, C.-S. Yoo, D. A. Young, *Phys. Rev. Lett.* **2002**, *88*, 135701.
[23] J. Etourneau, J. Potier, F. Ménil, *J. Alloys Compd.* **1992**, *188*, 1.
[24] J. M. McHale, A. Navrotsky, G. R. Kowach, V. E. Balbarin, F. J. DiSalvo, *Chem. Mater.* **1997**, *9*, 1538.
[25] F. K. Patterson, R. Ward, *Inorg. Chem.* **1966**, *5*, 1312.
[26] G. Bergerhoff, *Angew. Chem.* **1964**, *76*, 697.
[27] W. H. Baur, *Crystallogr. Rev.* **1987**, *1*, 59.
[28] O. Hassel, *Kristallchemie*, Verlag Theodor Steinkopff, Dresden und Leipzig, **1934**.
[29] S. V. Krivovichev, S. K. Filatov, *Acta Crystallogr. Sect. B* **1999**, *55*, 664.
[30] S. Alvarez, *Coord. Chem. Rev.* **1999**, *193–195*, 13.
[31] J. T. Anhaus, T. P. Kee, M. H. Schofield, R. R. Schrock, *J. Am. Chem. Soc.* **1990**, *112*, 1642.
[32] K. W. Given, L. H. Pignolet, *Inorg. Chem.* **1977**, *16*, 2982.
[33] P. Höhn, R. Kniep, A. Rabenau, *Z. Kristallogr.* **1991**, *196*, 153.
[34] D. A. Vennos, F. J. DiSalvo, *J. Solid State Chem.* **1992**, *98*, 318.
[35] A. Tennstedt, C. Röhr, R. Kniep, *Z. Naturforsch. B* **1993**, *48*, 794.
[36] M. G. Barker, M. J. Begley, P. P. Edwards, D. H. Gregory, S. E. Smith, *J. Chem. Soc. Dalton Trans.* **1996**, 1.
[37] T. Yamamoto, S. Kikkawa, F. Kanamaru, *J. Solid State Chem.* **1995**, *119*, 161.
[38] R. Hoppe, *Angew. Chem.* **1970**, *82*, 7; *Angew. Chem. Int. Ed. Engl.* **1970**, *9*, 25.
[39] D. D. Sarma, C. N. R. Rao, *J. Electron Spectrosc. Relat. Phenom.* **1980**, *20*, 25.
[40] J. A. T. Verhoeven, H. van Doveren, *Appl. Surf. Sci.* **1980**, *5*, 361.
[41] U. Steinbrenner, P. Adler, W. Hölle, A. Simon, *J. Phys. Chem. Solids* **1998**, *59*, 1527.
[42] G. Soto, W. de La Cruz, M. H. Farias, *J. Electron Spectrosc. Relat. Phenom.* **2004**, *135*, 27.
[43] N. Jansen, H. Spiering, P. Gütlich, D. Stahl, R. Kniep, V. Eyert, J. Kübler, P. C. Schmidt, *Angew. Chem.* **1992**, *104*, 1632; *Angew. Chem. Int. Ed. Engl.* **1992**, *31*, 1624.
[44] J. Weidlein, U. Müller, K. Dehnicke, *Schwingungsspektroskopie*, Thieme-Verlag, Stuttgart, **1988**.
[45] A. Earnshaw, B. N. Figgis, J. Lewis, R. D. Peacock, *J. Chem. Soc.* **1961**, 3132.
[46] W. Brenig, G. H. Döhler, H. Heyszenau, *Philos. Mag.* **1973**, *27*, 1093.
[47] A. A. Coelho, *J. Appl. Crystallogr.* **2003**, *36*, 86.
[48] H. M. Rietveld, *J. Appl. Crystallogr.* **1969**, *2*, 65.
[49] A. LeBail, H. Duroy, J. L. Fourquet, *Mater. Res. Bull.* **1988**, *23*, 447.
[50] R. W. Cheary, A. A. Coelho, J. P. Cline, *J. Res. Natl. Inst. Stand. Technol.* **2004**, *109*, 1.
[51] A. A. Coelho, *J. Appl. Crystallogr.* **2000**, *33*, 899.
[52] A. L. Spek, *J. Appl. Crystallogr.* **2003**, *36*, 7.
[53] R. Hundt, J. C. Schön, M. Jansen, *J. Appl. Crystallogr.* **2006**, *39*, 6.
[54] R. Dovesi, V. R. Saunders, C. Roetti, R. Orlando, C. M. Zicovich-Wilson, F. Pascale, B. Civalleri, K. Doll, N. M. Harrison, I. J. Bush, Ph. D′Arco, M. Llunell, *CRYSTAL06 User's Manual*, University of Torino, Torino, **2006**.
[55] A. Kokalj, *J. Mol. Graphics Modell.* **1999**, *17*, 176. Code available from http://www.xcrysden.org/.
[56] D. Andrae, U. Häussermann, M. Dolg, H. Stoll, H. Preuss, *Theor. Chim. Acta* **1990**, *77*, 123.
[57] M. Kaupp, P. von R. Schleyer, H. Stoll, H. Preuss, *J. Chem. Phys.* **1991**, *94*, 1360.
[58] A. Bergner, M. Doll, W. Küchle, H. Stoll, H. Preuss, *Mol. Phys.* **1993**, *80*, 1431.
[59] A. D. Becke, *J. Chem. Phys.* **1993**, *98*, 5648.
[60] J. P. Perdew, Y. Wang, *Phys. Rev. B* **1992**, *45*, 13244.

Received: June 6, 2008
Published online: August 29, 2008

 © 2008 Wiley-VCH Verlag GmbH & Co. KGaA, Weinheim